

Internal structure-mediated ultrafast energy transfer in self-assembled polymer-blend dots†

Cite this: *Nanoscale*, 2013, 5, 7265

Lei Wang,^a Chang-Feng Wu,^a Hai-Yu Wang,^{*a} Ya-Feng Wang,^b Qi-Dai Chen,^{*a} Wei Han,^b Wei-Ping Qin,^a Jason McNeill^c and Hong-Bo Sun^{ab}

Applications of polymeric semiconductors in organic electronics and biosensors depend critically on the nature of energy transfer in these materials. Important questions arise as to how this long-range transport degrades in amorphous condensed solids which are most amenable to low-cost optoelectronic devices and how fast energy transfer could occur. Here, we address these in disordered, densely packed nanoparticles made from green-light-harvesting host polymers (PFBT) and deep-red-emitting dopant polymers (PF-DBT5). By femtosecond selective excitation of donor (BT) units, we study in detail the internal structure-mediated energy transfer to uniformly distributed, seldom acceptor (DBT) units. It has been unambiguously demonstrated that the creation of interchain species is responsible for the limitation of bulk exciton diffusion length in polymer materials. This interchain Förster resonance energy transfer (FRET) becomes a preferred and dominant channel, and near 100% energy transfer efficiency could be achieved at high acceptor concentrations (>10 wt%). Side-chain carboxylic acid groups in functionalized polymer-blend dots slightly slow down the FRET rate, but it could not affect the Förster radius and FRET efficiency. These findings imply that a greater understanding of the role of interchain species could be an efficient approach to improve the cell efficiency.

Received 11th April 2013

Accepted 22nd May 2013

DOI: 10.1039/c3nr01817b

www.rsc.org/nanoscale

1 Introduction

Because of the unparalleled advantages of low cost and flexibility in broad application fields, π -conjugated polymers have received a great deal of attention.^{1–3} The performance of these organic devices and sensors is critically dependent on the nature of electronic energy transport in these materials.⁴ In particular, recent results indicate that molecular morphology strongly affects electronic energy transport in conjugated polymer materials.⁵ For example, single polymer chains or highly ordered aggregates of conjugated poly(2-methoxy-5-(2'-ethylhexyloxy)-1,4-phenylenevinylene) (MEH-PPV) exhibit ultra-long-range energy transfer distances of up to 60 nanometers,^{6,7} while the energy transfer length is only about 5 nm in amorphous bulk PPV-based films.⁸ Unraveling the degradation of the energy transport distance in bulk chaotic materials is particularly important, as it is a limiting factor for the efficiency of low-cost organic solar cells. Possible reasons for the energy transfer distance “shortening” are proposed including (i) creation of

interchain species that become low-energy trapping sites, (ii) higher disorder due to a greater range of orientations and (iii) energy levels arising from the chaotic packing of chains as they form solids.⁶ Nevertheless, identifying the roles played by each of these factors is still an open problem.

As demonstrated in previous reports,⁹ interchain energy transfer processes dominate in polymer films, because of the close contact between chains which favor interchain transport of the excited state, exhibiting a 1-order-of-magnitude increase in transfer rate compared to that of the polymer in a solution. But these energy transfer processes have been investigated primarily by means of ensemble spectroscopic measurements on bulk films.^{10,11} Ensemble measurements are not accurate, and sometimes misleading, because phase separation often occurs due to the inherent complexity and heterogeneity of polymer materials.¹² In order to investigate the energy transfer processes, the dopant molecules must be evenly dispersed within the host polymer. This is difficult to achieve in solid polymer blends, since it tends to form a micrometer-scale phase-separated morphology,^{13,14} which significantly affects the energy transfer and fluorescence properties.¹⁵ To overcome the problem, we investigated energy transfer processes in disordered, densely packed polymer-blend nanoparticles. These nanoparticles represent discrete nanoscale objects with uniformly distributed donor and acceptor units, which are not accessible in conjugated polymer films. Interchain energy transfer distance and time scales were obtained by femtosecond

^aState Key Laboratory on Integrated Optoelectronics, College of Electronic Science and Engineering, Jilin University, 2699 Qianjin Street, Changchun 130012, China. E-mail: haiyu_wang@jlu.edu.cn; hbsun@jlu.edu.cn

^bCollege of Physics, Jilin University, 119 Jiefang Road, Changchun 130023, China

^cDepartment of Chemistry, Clemson University, Clemson, South Carolina 29634, USA

† Electronic supplementary information (ESI) available: Calculation of the excitation density and solution of the fitting equation. See DOI: 10.1039/c3nr01817b

time-resolved fluorescence and theoretical modeling, which indicate fast, long-range energy funneling to the low-energy trapping species.

Conjugated polymer nanoparticles have exhibited interesting photophysics and high fluorescence brightness for biological imaging.^{16–20} The nanoparticles in this study were made from a green-light-harvesting polymer PFBT as donor and a deep-red emitting polymer PF-DBT5 as acceptor (Fig. 1a). We chose the two polymer components because the blended polymer nanoparticles exhibit large absorption cross-sections in the blue region due to the BT units (donor units), and highly bright, deep-red fluorescence of DBT units (acceptor units, playing the role of interchain species here). In this model system, pumping the absorption of BT units (~ 460 nm) results in unambiguous interchain energy transfer to the low-energy emissive sites (DBT units). On the other hand, the low fraction of the PF-DBT5 polymer as well as the low molar ratio of DBT to fluorene units guarantees that the low-energy quenching sites not only can exactly evaluate the amount, but also are evenly distributed in the nanoparticles. This strategy results in a well controlled system with donors and acceptors evenly dispersed in the nanoscale domains, which are hardly obtained from bulk film fabrication. Fig. 1b shows the absorption spectra of the pure and blended polymer nanoparticles. For the polymer blend nanoparticles, the ratio of the two absorption peaks varied with the increasing weight fraction of the PF-DBT5 dopant polymer. For 10% weight fraction, the fluorescence of the PFBT donor (~ 550 nm) was almost completely quenched, accompanied by the strong emission (peak at 640 nm) of the PF-DBT5 acceptor (Fig. 1c). The typical diameter of the nanoparticles employed here was in the range of 30–40 nm, as indicated by dynamic light scattering measurements (ESI, Fig. S1†). As a result, in the

case of 10% weight fraction, each polymer nanoparticle comprised ~ 20 PF-DBT5 polymer molecules, each of which consisted of only ~ 6 DBT units randomly distributed along the polymer chain. Moreover, because the formation of polymer nanoparticles is driven by folding and torsion of the polymer backbone through hydrophobic interactions in a rapid solvent mixing process, these nanoparticles possess a glassy disordered morphology, as shown by polyfluorene (PF) nanoparticles in a previous report.²¹

2 Experiments

The semiconducting polymer nanoparticles were prepared from the three polymers (PFBT, PFBT-C14 and PF-DBT5, respectively) by using the reprecipitation method. All experiments were performed at room temperature unless indicated otherwise.¹⁹ PFBT was purchased from American Dye Source, Inc. PFBT-C14 and PF-DBT5 were synthesized as in previous reports.^{20,25} PFBT nanoparticles were prepared by injecting 2 mL ($50 \mu\text{g mL}^{-1}$) of tetrahydrofuran (THF) stock solution of the PFBT polymer into 10 mL of Milli-Q water under ultrasonication. PFBT-C14 nanoparticles were prepared by injecting 2 mL ($50 \mu\text{g mL}^{-1}$) of THF stock solution of the PFBT-C14 polymer into 10 mL of Milli-Q water under ultrasonication. PF-DBT5 nanoparticles were prepared by injecting 2 mL ($50 \mu\text{g mL}^{-1}$) of tetrahydrofuran (THF) stock solution of the PF-DBT5 polymer into 10 mL of Milli-Q water under ultrasonication. The THF was removed by nitrogen stripping.

Blended nanoparticles in aqueous solution were prepared by using a modified nano-precipitation method.²⁰ In a typical preparation, the light-harvesting polymer PFBT (or PFBT-C14) and red-emitting polymer PF-DBT5 were first dissolved in THF to make a 1 mg mL^{-1} stock solution, respectively. The two polymer solutions were diluted and mixed in THF to produce a solution mixture with a PFBT (or PFBT-C14) concentration of $500 \mu\text{g mL}^{-1}$ and a PF-DBT5 concentration of $5 \mu\text{g mL}^{-1}$ (or $15 \mu\text{g mL}^{-1}$). The mixture was sonicated to form a homogeneous solution. A 2 mL quantity of the solution mixture was quickly added to 10 mL of Milli-Q water in a vigorous bath sonicator. The THF was removed by nitrogen stripping. The solution was concentrated by continuous nitrogen stripping to 5 mL on a 90°C hotplate followed by filtration through a 0.2 micron filter for femtosecond time-resolved fluorescence experiments. These nanoparticle dispersions were clear and stable for months without signs of aggregation.

Time-resolved fluorescence experiments: nanosecond fluorescence lifetime experiments were performed by a time-correlated single-photon counting (TCSPC) system under right-angle sample geometry. A 405 nm picosecond diode laser (Edinburgh Instruments EPL375, repetition rate 2 MHz) was used to excite the samples. The fluorescence was collected by a photomultiplier tube (Hamamatsu H5783p) connected to a TCSPC board (Becker&Hickel SPC-130). The time constant of the instrument response function (IRF) was about 300 ps.

Subpicosecond time resolved emission was measured by the femtosecond fluorescence upconversion method. A mode-locked Ti:sapphire laser/amplifier system (Solstice, Spectra-Physics) was used. The output of the amplifier of 1.5 mJ pulse

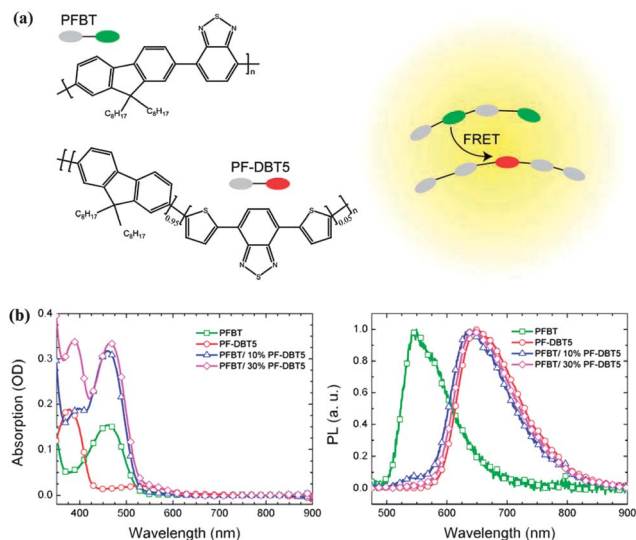


Fig. 1 Preparation and steady-state spectroscopy of PFBT/PF-DBT5 nanoparticles. (a) Schematic illustration of polymer-blend nanoparticles. The grey, green and red ellipse represent the polyfluorene units (PF), donor BT units and the interchain species-acceptor DBT units, respectively. Steady-state absorption (b) and normalized emission spectra (c) of pure and blended polymer nanoparticles in water under 460 nm excitation.

energy, 100 fs pulse width, at 800 nm wavelength is split into two parts; through a TOPAS system, the stronger beam was used to generate excitation light at 460 nm. The sample was stored in a 2 mm cuvette, which was rigorously stirred with a magnetic stirrer to avoid degradation. The resultant fluorescence was collected and focused onto a 1 mm thick BBO crystal with a cutting angle of 35 degrees. The other part of the RGA output was sent into an optical delay line and served as the optical gate for the upconversion of the fluorescence. The generated sum frequency light was then collimated and focused into the entrance slit of a 300 mm monochromator. A UV-sensitive photomultiplier tube 1P28 (Hamamatsu) was used to detect the signal. The FWHM of the instrument response function was about 400 fs. Samples were rigorously stirred with a magnetic stirrer for all of the femtosecond fluorescence dynamics experiments.

3 Results and discussion

To scrutinize the time and distance scales of the energy transfer process, femtosecond time-resolved fluorescence dynamics were investigated by the femtosecond fluorescence upconversion technique. First, we investigated the excitation intensity-dependent femtosecond fluorescence dynamics in host polymer PFBT nanoparticles (Fig. 2). The suitable excitation wavelength was fixed at 460 nm, corresponding to the absorption of BT units as stated above. Unless indicated otherwise, samples were rigorously stirred with a magnetic stirrer to avoid degradation in all the femtosecond fluorescence dynamics experiments. These polymer nanoparticles exhibited carrier density-dependent transient behaviors, which were similar to the bulk polyfluorene films, due to the diffusion-controlled exciton–exciton annihilation.²²

We adopted a three-dimensional (3D) diffusion model as described previously,²³ to fit these transient decay traces (see details in the ESI†). Based on the estimated exciton density, the

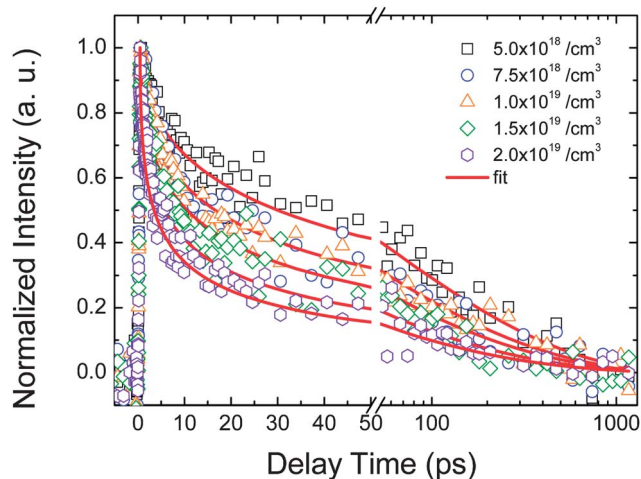


Fig. 2 Femtosecond time-resolved fluorescence for PFBT polymer nanoparticles. Intensity-dependent PL dynamics probed at 550 nm at 460 nm excitation. Red solid lines represent the fitting results by a 3D diffusion model.

global fitting of all five kinetic curves gives two satisfactory fitting parameters together: one is the exciton–exciton annihilation radius, $R_a = 4.0 \pm 0.2$ nm; the other is the isotropic diffusion constant, $D = (2.7 \pm 0.3) \times 10^{-4}$ cm² s⁻¹. Considering the exciton lifetime τ_1 of 540 ps determined by the time-correlated single photon counting (TCSPC) technique (ESI, Fig. S2 and Table S1†), the diffusion length and annihilation rate constant were then estimated to be $L_D = \sqrt{D\tau_1} = 3.8 \pm 0.3$ nm and $\gamma = 4\pi R_a D = 1.35 \times 10^{-9}$ cm² s⁻¹, respectively. These parameters are consistent with those in PFBT (also named F8BT) films.²⁴ Our results suggest that higher disorder due to a greater range of orientations such as in the case of polymer nanoparticles could not decrease the intrachain exciton diffusion length.

Next, PFBT nanoparticles were blended with a small amount of the PF-DBT5 acceptor polymer. For a 10% weight fraction, there were uniformly distributed ~ 120 acceptor units per nanoparticle on an average, surrounded by thousands of randomly distributed donor units. To verify our speculation, femtosecond time-resolved fluorescence quenching experiments probed at 550 nm in the blended nanoparticles were performed. In order to decrease the influence of carrier density on decay kinetics, the lowest excitation intensity in the detectable signal range was adopted. As shown in Fig. 3a, the decay traces of donor emission decreased remarkably faster than that of pure PFBT nanoparticles. Within the first 100 ps, the donor emission decayed completely, and it was faster for higher acceptor concentrations. The temporal evolution of acceptor emission probed at 640 nm provides complementary evidence for energy transfer from the host to dopant polymers. Both temporal evolution traces at the blending ratio of 10% and 30%

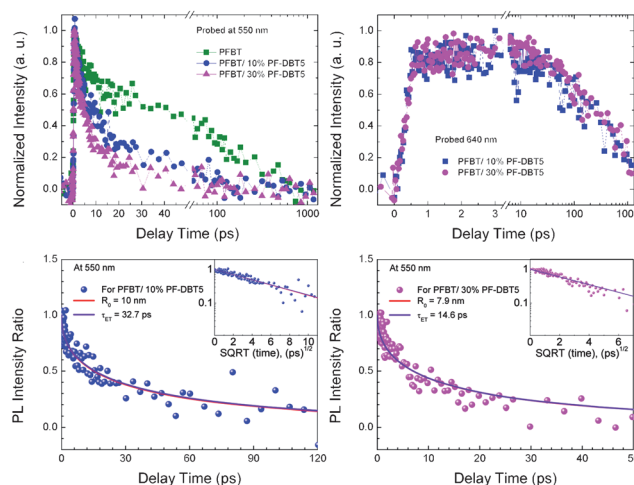


Fig. 3 Femtosecond time-resolved fluorescence and theoretical modeling for blended PFBT/PF-DBT5 nanoparticles. Normalized PL dynamics for blended nanoparticles under 460 nm excitation (5 nJ per pulse) probed at 550 nm for donor PL quenching (a) and probed at 640 nm for acceptor emission (b). (c and d) Modeling the PL intensity ratio for blended nanoparticles with different dopant fractions. The solid lines represent the fitting results, which give the Förster radius (R_0) and resonance energy transfer time (τ_{ET}), respectively. Insets show the PL intensity ratio on a logarithmic scale as a function of the square root of time.

exhibited a flat stage up to 10 ps following a fast rising within the first 3 ps, and then began to decay (Fig. 3b). The emission of the acceptors correlated well with the fluorescence quenching of the donor, supporting fast energy transfer in these blended nanoparticles.

To quantitatively analyze this process, two consistent models based on Förster resonance energy transfer were used to fit the PL quenching dynamics (see ESI†), which describe the same physical process from the angle of Förster energy transfer time τ_{ET} and radius R_0 , respectively. Fig. 3c and d show the modeling results for blended particles with different fractions of the dopant molecules. The fitting curves described by the Förster resonance energy transfer theory are in excellent agreement with experimental data in the entire decay traces. In the plots of PL intensity ratio on a logarithmic scale as a function of the square root of time (insets of Fig. 3c and d), a linear dependence between the theoretical and experimental data was clearly observed, consistent with the prediction of Förster models. The resulting FRET times were estimated to be about 32.7 ps and 14.6 ps for the blending ratio of 10% and 30%, respectively. Considering that the average PL lifetime (τ_{ave} in ESI Table S1†) for pure PFBT polymer nanoparticles was 0.68 ns, the corresponding energy transfer efficiency ($\eta_{ET} = 1 - \tau_{ET}/\tau_{ave}$) was estimated to be as high as 95% and 98%, respectively. Such highly efficient interchain energy transfer also rules out the possibility of incomplete or multiple energy transfer processes. The fitting result gave the Förster radii of 10 nm for PFBT/10 wt% PF-DBT5 and 7.9 nm for PFBT/30 wt% PF-DBT5 nanoparticles, respectively. In a word, this long-range energy transfer distance is sufficiently large to break the ultra-long energy transfer path in a single polymer chain into pieces of nanometers if any low-energy trapping site exists nearby.

We further examined the energy transfer processes in blended nanoparticles with reduced interchain interactions. As described in a recent report,²⁵ a portion of ionic groups such as carboxylic acid were covalently attached to the side chains of the PFBT polymer. It could lead to some energy levels arising from the chaotic packing of chains. On the other hand, the hydrophilic side chains can swell the particles and result in a somewhat loosely aggregated morphology of polymer chains. As a result, we could check the effect of chaotic packing of chains, and we could also expect that the energy transfer rate in such nanoparticles may slow down because of the reduced interchain interactions (increased donor–acceptor distance). Pure and blended nanoparticles were prepared from a PFBT polymer with side-chain carboxylic acid groups at a molar fraction of 14% (PFBT-C14 for short, molecular structure in ESI Fig. S4†). The steady-state optical spectra and intensity-dependent femto-second fluorescence dynamics are presented in ESI Fig. S5.† Compared with the pure PFBT nanoparticles without side-chain hydrophilic groups, PFBT-C14 nanoparticles showed a smaller exciton–exciton annihilation radius $R_a = 3.1 \pm 0.5$ nm, and larger isotropic diffusion constant $D = (3.7 \pm 0.4) \times 10^{-4}$ cm² s⁻¹. Correspondingly, the PFBT-C14 nanoparticles exhibited a larger exciton diffusion length $L_D = \sqrt{D\tau_1} = 5.1 \pm 0.4$ nm ($\tau_1 = 710$ ps for PFBT-C14 nanoparticles, see ESI Table S1†) and a comparable annihilation rate constant ($\gamma = 4\pi R_a D = 1.44 \times$

10^{-9} cm² s⁻¹). The decreased exciton–exciton annihilation radius is due to the increment of chaotic packing of chains in the PFBT-C14 nanoparticles, while the increased exciton diffusion length is consistent with the reduced interchain interactions. This suggests that the energy levels arising from the chaotic packing of chains are not yet the main reason for the degradation of the exciton diffusion length in solid polymer materials. For the PFBT-C14/30 wt% PF-DBT5 blended nanoparticles, the interchain energy transfer from BT donors to DBT acceptors was observed more clearly because the energy transfer time was increased (Fig. 4a). Accompanied by the quenching of donor emission, the acceptor fluorescence dynamics exhibited a long rising up to first 10 ps, and then began to decay until nearly 100 ps. The emission dynamics of the acceptors can be well reproduced with a multiexponential fitting, which gives a rising of ~ 16 ps (ESI, Fig. S6†). Moreover, the quenching dynamics of the donor emission were analyzed using the same method as

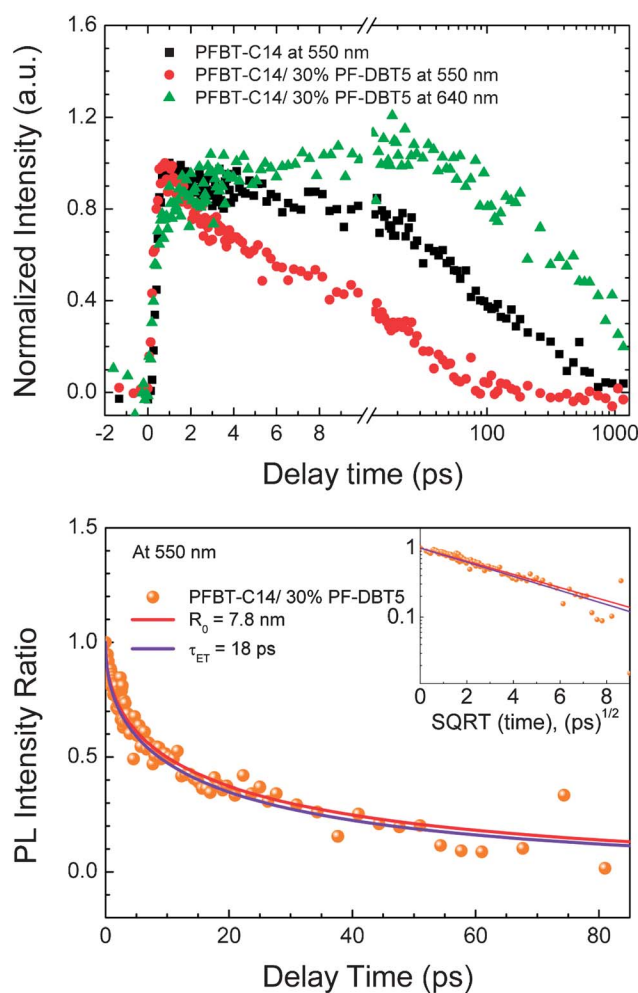


Fig. 4 Femtosecond time-resolved fluorescence and theoretical modeling for blended PFBT-C14/30% PF-DBT5 nanoparticles. (a) PL dynamics for pure PFBT-C14 nanoparticles and blended PFBT-C14/30% PF-DBT5 nanoparticles under 460 nm excitation (5 nJ per pulse). (b) Modeling the PL intensity ratio for blended PFBT-C14/30% PF-DBT5 nanoparticles. The solid lines represent the fitting results. The inset is the PL intensity ratio on a logarithmic scale as a function of the square root of time.

stated above (Fig. 4b), which resulted in a longer FRET time $\tau_{\text{ET}} = 18$ ps as well as a comparable Förster radius $R_0 = 7.8$ nm. Considering the average PL lifetime (~ 0.86 ns) of PFBT-C14 nanoparticles (ESI, Table S1†), the efficiency of interchain energy transfer remained as high as $\sim 98\%$.

The internal structure-mediated FRET parameters obtained from our investigations are presented in Fig. 5. It shows that the FRET time is strongly dependent on the dopant fraction, showing fast energy transfer dynamics as the blending ratio increases. Nearly 100% intra-particle energy transfer efficiency could be achieved at higher acceptor concentrations (>10 wt%, or >120 acceptor units per nanoparticle). However, the Förster radius exhibited weak dependence on the concentration of the acceptor units as well as the morphology of the donor chains, indicating an ideal system for exploring the ultrafast energy transfer process in conjugated polymers. Therefore, our investigations on these blended nanoparticles provide accurate information about the time and distance scale of energy transfer in disordered solid-state conjugated polymers. The femtosecond time-resolved measurement in this work, as well as steady-state fluorescence spectroscopy studies,²⁶ strongly suggests that the creation of interchain species (here the role of DBT units) leads to an effective energy funneling to the low-energy trapping sites. Such an efficient exciton quenching would limit the bulk exciton diffusion length in disordered conjugated polymer films. Hence, as we already know, the ultra-long exciton diffusion distance in single polymer chains is hard to reproduce in solid polymer blends.

The relatively long-range interaction between donor and acceptor units makes sure that the influence of polymer molecular aggregation and functionalization could not be effective competing mechanisms. This suggests that more functionalization could be introduced into the polymer-blend dots for different applications. It also strongly implies that if some chemical impurities²⁷ play the role of interchain species in polymer systems, it could be one of the important factors limiting the performance of plastic solar cells. Thus, a greater

understanding of the role of interchain species, and how to control them by the internal structure-mediated energy transfer mechanism, could be an efficient approach to improve the cell efficiency. In addition, taking advantage of the randomly distributed spatial structure of donor and acceptor units like in the case of polymer-blend dots, high efficiency of energy collection also might be achieved in uniform polymer systems, compared with the natural process of light harvesting.^{28,29}

4 Conclusions

Our findings unambiguously indicate that the creation of interchain species is responsible for the degradation of the bulk exciton diffusion length in polymer materials. It provides a clear picture on the distance and time scales of energy transfer to the interchain quenching species in PFBT/PF-DBT5 polymer-blend dots. The efficient quenching (nearly 100%) can be described by the Förster transfer model with a Förster radius of ~ 10 nm, 2 to 3 times larger than the exciton–exciton annihilation radius (~ 4 nm) in the pure host polymer. The energy transfer time is in the range of ten picoseconds, which is dependent on the density of interchain species. This study emphasizes that these results on interchain energy transfer are not only limited to these nanoparticles, but also can be generalized to other conjugated polymer systems. It will be helpful for understanding the photophysics of conjugated polymers and facilitating the development of organic solar cells based on polymer materials.

Acknowledgements

The authors would like to acknowledge the 863 project of China Grant no. 2013AA030902 and Natural Science Foundation, China (NSFC) under Grant no. 20973081, 21273096, 60525412, 60677016 and 10904049 for support. C. F. Wu acknowledges the support of One-Thousand Talents program in China and NSFC under Grant no. 612220144.

Notes and references

- 1 C. D. Müller, A. Falcou, N. Reckfuss, M. Rojahn, V. Wiederhirn, P. Rudati, H. Frohne, O. Nuyken, H. Becker and K. Meerholz, *Nature*, 2003, **421**, 829.
- 2 J. Peet, A. J. Heeger and G. C. Bazan, *Acc. Chem. Res.*, 2009, **42**, 1700.
- 3 S. W. Thomas, G. D. Joly and T. M. Swager, *Chem. Rev.*, 2007, **107**, 1339.
- 4 C. Bardeen, *Science*, 2011, **331**, 544.
- 5 X. N. Yang and J. Loos, *Macromolecules*, 2007, **40**, 1353.
- 6 J. C. Bolinger, M. C. Traub, T. Adachi and P. F. Barbara, *Science*, 2011, **331**, 565.
- 7 J. Vogelsang, T. Adachi, J. Brazard, D. A. V. Bout and P. F. Barbara, *Nat. Mater.*, 2011, **10**, 942.
- 8 D. E. Markov, E. Amsterdam, P. W. M. Blom, A. B. Sieval and J. C. Hummelen, *J. Phys. Chem. A*, 2005, **109**, 5266.
- 9 D. Beljonne, G. Pourtois, C. Silva, E. Hennebicq, R. H. Friend, G. D. Scholes, S. Setayesh, K. Müllen and J. L. Brédas, *Proc. Natl. Acad. Sci. U. S. A.*, 2002, **99**, 10982.

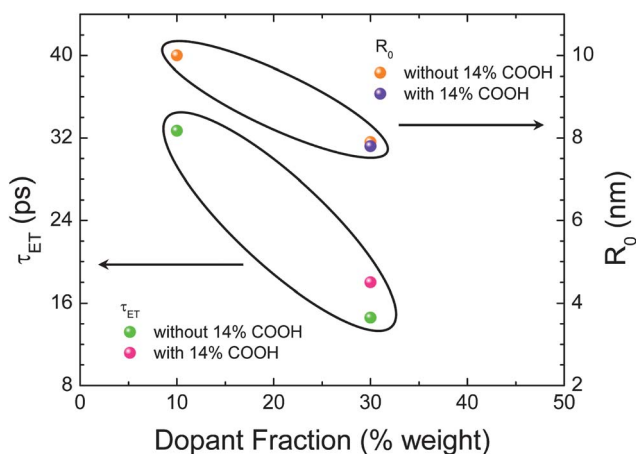


Fig. 5 Summary of FRET time and distance of in blended PFBT/PF-DBT5 nanoparticles. Resonance energy transfer time (τ_{ET}) and Förster radius (R_0) were extracted from models as a function of dopant percentage.

- 10 A. Dogariu, D. Vacar and A. J. Heeger, *Phys. Rev. B: Condens. Matter Mater. Phys.*, 2001, **58**, 10218.
- 11 C. R. McNeill, S. Westenhoff, C. Groves, R. H. Friend and N. C. Greenham, *J. Phys. Chem. C*, 2007, **111**, 19153.
- 12 J. L. Brédas, J. E. Norton, J. Cornil and V. Coropceanu, *Acc. Chem. Res.*, 2009, **42**, 1691.
- 13 A. C. Arias, J. D. MacKenzie, R. Stevenson, J. J. M. Halls, M. Inbasekaran, E. P. Woo, D. Richards and R. H. Friend, *Macromolecules*, 2001, **34**, 6005.
- 14 T. Kietzke, D. Neher, K. Landfester, R. Montenegro, R. Güntner and U. Scherf, *Nat. Mater.*, 2003, **2**, 408.
- 15 J. Chappell, D. G. Lidzey, P. C. Jukes, A. M. Higgins, R. L. Thompson, S. O'Connor, I. Grizzi, R. Fletcher, J. O'Brien, M. Geoghegan and R. A. L. Jones, *Nat. Mater.*, 2003, **2**, 616.
- 16 P. E. Palacios, F. R. F. Fan, J. K. Grey, J. Suk, A. J. Bard and P. F. Barbara, *Nat. Mater.*, 2007, **6**, 680.
- 17 E. Collini and G. D. Scholes, *Science*, 2009, **323**, 369.
- 18 J. B. Yu, C. F. Wu, Z. Y. Tian and J. McNeill, *Nano Lett.*, 2012, **12**, 1300.
- 19 C. F. Wu, B. Bull, C. Szymanski, K. Christensen and J. McNeill, *ACS Nano*, 2008, **2**, 2415.
- 20 C. F. Wu, S. J. Hansen, Q. Hou, J. B. Yu, M. Zeigler, Y. H. Jin, D. R. Burnham, J. D. McNeill, J. M. Olson and D. T. Chiu, *Angew. Chem., Int. Ed.*, 2011, **50**, 3430.
- 21 C. F. Wu and J. McNeill, *Langmuir*, 2008, **24**, 5855.
- 22 P. E. Shaw, A. Ruseckas, J. Peet, G. C. Bazan and I. D. W. Samuel, *Adv. Funct. Mater.*, 2010, **20**, 155.
- 23 H. Wang, H. Y. Wang, B. R. Gao, L. Wang, Z. Y. Yang, X. B. Du, Q. D. Chen, J. F. Song and H. B. Sun, *Nanoscale*, 2011, **3**, 2280.
- 24 M. A. Stevens, C. Silva, D. M. Russell and R. H. Friend, *Phys. Rev. B: Condens. Matter Mater. Phys.*, 2001, **63**, 165213.
- 25 X. J. Zhang, J. B. Yu, C. F. Wu, Y. H. Jin, Y. Rong, F. M. Ye and D. T. Chiu, *ACS Nano*, 2012, **6**, 5429.
- 26 C. F. Wu, H. S. Peng, Y. F. Jiang and J. McNeill, *J. Phys. Chem. B*, 2006, **110**, 14148.
- 27 T. Y. Chu, J. P. Lu, S. Beaupré, Y. G. Zhang, J. R. Pouliot, J. Y. Zhou, A. Najari, M. Leclerc and Y. Tao, *Adv. Funct. Mater.*, 2012, **22**, 2345.
- 28 E. Collini, C. Y. Wong, K. E. Wilk, P. M. G. Curmi, P. Brumer and G. D. Scholes, *Nature*, 2010, **463**, 644.
- 29 H. Dong, D. Z. Xu, J. F. Huang and C. P. Sun, *Light: Sci. Appl.*, 2012, **1**, e2.